

Development of a hydrogen peroxide-responsive and oxygen-carrying nanoemulsion for photodynamic therapy against hypoxic tumors using phase inversion composition method

Liang Hong, Jia Zhang, Junxian Geng, Junle Qu and Liwei Liu*

*Key Laboratory of Optoelectronic Devices
and Systems of Ministry of Education and Guangdong Province
College of Optoelectronic Engineering
Shenzhen University, Shenzhen 518060, P. R. China
liulw@szu.edu.cn

Received 26 August 2020

Accepted 23 November 2020

Published 23 December 2020

Photodynamic therapy (PDT) has become an attractive tumor treatment modality because of its noninvasive feature and low side effects. However, extreme hypoxia inside solid tumors severely impedes PDT therapeutic outcome. To overcome this obstacle, various strategies have been developed recently. Among them, *in situ* oxygen generation, which relies on the decomposition of tumor endogenous H₂O₂, and oxygen delivery tactic using high oxygen loading capacity of hemoglobin or perfluorocarbons, have been widely studied. The *in situ* oxygen generation strategy has high specificity to tumors, but its oxygen-generating efficiency is limited by the intrinsically low tumor H₂O₂ level. In contrast, the oxygen delivery approach holds advantage of high oxygen loading efficiency, nevertheless lacks tumor specificity. In this work, we prepared a nanoemulsion system containing H₂O₂-responsive catalase, highly efficient oxygen carrier perfluoropolyether (PFPE), and a near-infrared (NIR) light activatable photosensitizer IR780, to combine the high tumor specificity of the *in situ* oxygen generation strategy and the high efficiency of the oxygen delivery strategy. This concisely prepared nanoplateform exhibited enhanced and H₂O₂-controllable production of singlet oxygen under light excitation, satisfactory cytocompatibility, and ability to kill cancer cells under NIR light excitation. This highlights the potential of this novel nanoplateform for highly efficient and selective NIR light mediated PDT against hypoxic tumors. This research provides new insight into the design of intelligent nanoplateform for relieving tumor hypoxia and enhancing the oxygen-dependent PDT effects in hypoxic tumors.

Keywords: Hypoxia; catalase; oxygen delivery; perfluorocarbon; near-infrared.

*Corresponding author.

1. Introduction

Photodynamic therapy (PDT) has become a powerful tool to treat tumors, owing to its noninvasiveness, high anatomical precision, and low side effects. In a typical PDT process, photosensitizers are exposed to light and convert oxygen to cytotoxic reactive oxygen species (ROS), resulting in destruction of tumor cells.¹ Nonetheless, the therapeutic efficacy of PDT is severely limited by the hypoxic microenvironment in solid tumors.² Hypoxia is an important hallmark of solid tumors that has drawn increasing attention. The intrinsic hypoxia results from rapid proliferation of tumor cells and abnormal structure of tumor vessels.^{3,4} Moreover, the hypoxia is exacerbated during the PDT process, as plenty of oxygen is consumed.⁵ Particularly, it has been widely recognized that tumor hypoxia not only impairs the efficiency of PDT, but also promotes proliferation, angiogenesis, and metastasis of tumors.⁶ Therefore, it is urgent to develop strategies to overcome this obstacle.

To address tumor hypoxia, a lot of pioneering efforts have been devoted. Till date, two pathways to overcome tumor hypoxia have been highlighted. One is oxygen-independent PDT, and the other is tumor oxygenation. The oxygen-independent PDT utilizes methods such as type I PDT and Fenton reaction to generate ROS in absence of oxygen.^{7,8} Although effective, oxygen-independent PDT does not truly change the tumor hypoxic microenvironment, leaving hypoxia-related issues such as inadequate blood supply and drug-resistant gene expression unresolved.^{9,10} In contrast, tumor oxygenation has drawn intensive attention because of its ability to alter tumor hypoxic microenvironment.

Nowadays, typical tumor oxygenation approaches include (1) *in situ* oxygen generation and (2) oxygen delivery. Elevated H₂O₂ level is another feature of the tumor microenvironment compared with normal tissues.^{11,12} One of the most widely studied *in situ* oxygen generation strategies is degradation of exogenous MnO₂ which could be accelerated by the H₂O₂ in the tumor site.¹³ The acidity of the tumor microenvironment induces degradation of MnO₂, which forms Mn²⁺, water, and oxygen. This degradation is accelerated by the H₂O₂ rich in tumor tissues.¹⁴ However, the toxicity of Mn²⁺ generated after the decomposition is a safety concern.¹⁵ An alternative method is catalysis of

tumor endogenous H₂O₂ decomposition using catalase.¹⁶ In living organisms, catalase is an important enzyme which can protect cells from oxidative damage through catalyzing the decomposition of H₂O₂ into water and oxygen. As a biological catalyst, the catalytic efficiency of catalase is higher than that of inorganic catalysts such as MnO₂ and Fe₂O₃.¹⁷⁻¹⁹ The *in situ* oxygen generation strategies hold the advantage of high tumor specificity.²⁰ Nevertheless, the oxygen-generating efficiency of these approaches is low, due to the small amount of H₂O₂ available in tumors.^{21,22}

On the other hand, oxygen delivery tactics rely typically on oxygen transportation by hemoglobin or perfluorocarbon-based carriers.²³ Hemoglobin-based nanomaterials have been shown to relieve tumor hypoxia and boost the efficiency of PDT.²⁴ Nevertheless, free hemoglobin in circulation may cause side effects such as kidney tubule damage.²⁵ Meanwhile, the insufficient oxygen loading capacity of hemoglobin impedes its application. In contrast, perfluorocarbon-based oxygen carriers have excellent biocompatibility and robust oxygen loading capacity.²⁶ At 25°C under 1 atm, perfluorocarbons can carry approximately twice amount of oxygen as blood can.²² In addition, it was reported that perfluorocarbon could reserve ROS and enormously extend its lifetime.¹⁰ However, the oxygen delivery strategy has inferior tumor selectivity compared with *in situ* oxygen generation tactic.

In this research, we introduce an oxygen-enriching strategy that combines the high tumor selectivity of *in situ* oxygen generation tactic and the high ROS generation efficiency of oxygen delivery approach. We designed and prepared a nanoemulsion system including H₂O₂-responsive catalase, high oxygen loading efficiency carrier PFPE, and a near-infrared (NIR) photosensitizer IR780, which was termed as CIPN, in abbreviation for catalase@IR780-PFPE/water nanoemulsion (Fig. 1). This nanoplateform offers the opportunity for highly selective and efficient NIR light activated PDT for hypoxic tumors. Moreover, to avoid the catalase activity loss, toxicity, and tediousness caused by routine chemical synthetic preparation approach, we created the nanoplateform using a mild, toxic reagent-free, and simple phase inversion composition (PIC) method, which may facilitate the industrialization and clinical translation of PDT.

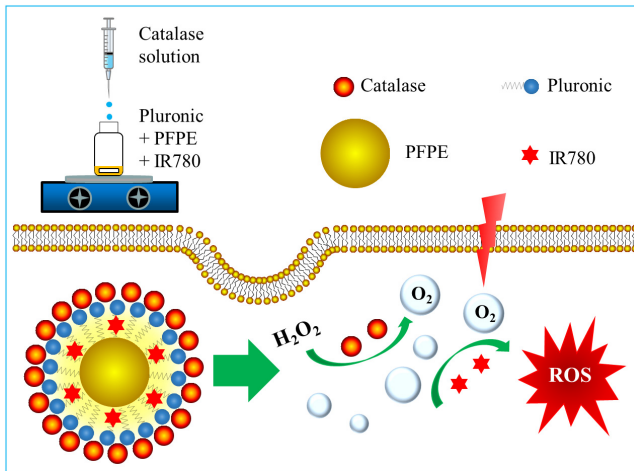


Fig. 1. Schematic illustration of the preparation method of the nanoparticle and the enhanced NIR light activatable PDT for hypoxic tumors.

2. Materials and Methods

2.1. Materials

Catalase powder was obtained from Merck (Kenilworth, US). 95% IR780 iodide was provided by Bailingwei (Beijing, China). PFPE (Fluorolink® MD700) was bought from Solvay (Brussels, Belgium). Pluronic (Mn 2900) and dimethyl sulfoxide (DMSO) were purchased from Aladdin (Shanghai, China). 1,3-diphenylisobenzofuran (DPBF) was bought from TCI (Tokyo, Japan). Cell counting kit-8 (CCK-8) was provided by Dojindo Laboratories (Kumamoto, Japan). 30% H_2O_2 was obtained from Xilong Scientific, Shantou, China. Double distilled water was used throughout the experiments.

2.2. Preparation of CIPN

The CIPN preparation was carried out using PIC method at 25°C without exposure to light. First, 0.01 g IR780, 0.7 g Pluronic 2900 and 0.3 g PFPE were bath sonicated for 10 min and then mixed for 1.5 h at 1250 r min⁻¹. Afterwards, 9 mL of 0.02% catalase solution was added dropwise (120 drops per minute) to the mixture under stirring at 1250 r min⁻¹. Then, the stirring was continued for 0.5 h. In the end, the liquid was filtered with a 0.45 µm syringe filter (Millipore, Bedford, US). For comparison, IR780-PFPE/water nanoemulsion (IPN) was prepared as CIPN except that catalase was absent. PFPE/water nanoemulsion (PN) was prepared as CIPN except that catalase and IR780 were absent.

2.3. Characterization of CIPN

The droplet size distributions of nanoemulsions were determined using a dynamic light scattering instrument (Nano Brook 90 Plus Zeta, Brookhaven Instruments, Holtsville, US) at 25°C. Prior to measurements, the nanoemulsions were diluted 10 times with water. The refractive index employed was 1.33. The zeta potential measurements were performed using a Nano Brook 90 Plus Zeta (Brookhaven Instruments, Holtsville, US) at 25°C. The morphology of the nanoemulsion droplets was detected with a transmission electron microscope (TEM) JEM-1230 (Nippon Tekno, Osaka, Japan). A drop of CIPN was placed onto a copper grid and dried prior to examination with TEM. The absorption spectra were recorded on a UV1780 spectrophotometer (Shimadzu, Shanghai, China) at 25°C. To investigate the physiological stability, the CIPNs were diluted 30 times with RPMI 1640 culture medium, and stored at 25°C or 37°C. The mean droplet diameters of the CIPNs were measured at predetermined time points.

2.4. Photodynamic efficacy

The singlet oxygen (1O_2) production was measured using a specific 1O_2 probe DPBF. Five treatment groups were set, including (1) Water, (2) H_2O_2 , (3) IPN + H_2O_2 , (4) CIPN + Water, and (5) CIPN + H_2O_2 . IPN or CIPN was diluted with 100 mmol L⁻¹ H_2O_2 or water to the same IR780 concentration (indicated by the absorbance at

780 nm) to obtain the IPN + H₂O₂, CIPN + Water, or CIPN + H₂O₂ group samples. Then, 50 μL freshly prepared DPBF (1 mg mL⁻¹) in DMSO was added to 3 mL water, H₂O₂ (100 mmol L⁻¹), or the as-prepared samples and mixed together. Afterwards, the samples were irradiated with NIR laser (808 nm, 2 W cm⁻²) generated from an MDL-III-808-2.5W laser device (Changchun New Industries Optoelectronics Technology Co., Ltd., Changchun, China) for 10 s. The absorbances at 410 nm prior to and past irradiation were measured using a UV1780 spectrophotometer (Shimadzu, Shanghai, China) and normalized.²⁷ All operations were carried out in a dark room without light exposure.

2.5. Cell culture

OVCAR-3 cells (ovarian cancer cells) were provided by American Type Culture Collection (ATCC, Manassas, US). The cells were cultivated in RPMI 1640 medium supplemented with 10% fetal bovine serum and 1% streptomycin/penicillin at 37°C in a humidified atmosphere with 5% CO₂.

2.6. Cytocompatibility assay

OVCAR-3 cells were seeded in 96-well plates at a density of 1.5×10^4 cells per well and allowed to grow at 37°C, 5% CO₂ for 24 h. CIPNs were diluted to a series of concentrations by serum-free medium. Then, the cells were incubated with different concentrations of CIPNs at 37°C, 5% CO₂ for 24 h. Cells incubated with serum-free medium were used as control. Subsequently, the liquids in the plates were withdrawn, and the mixed solution consisting of CCK-8 (10 μL) and serum-free medium (90 μL) was added into each well. Afterwards, the cells were incubated at 37°C for 1 h, and the absorbance intensity at 450 nm was detected with a Microplate Reader (RT-6100, Rayto Life and Analytical Sciences, Shenzhen, China) after shaking for 2 min, using 630 nm as reference wavelength.

2.7. In vitro PDT

OVCAR-3 cells were seeded in 96-well plates at a density of 1.5×10^4 cells/well and incubated at 37°C, 5% CO₂ for 24 h. Afterwards, the cells were incubated with CIPNs (800 μg mL⁻¹, diluted with serum-free medium) at 37°C for 10 h. Afterwards,

the CIPN dispersions were changed for serum-free medium, and the cells were irradiated with NIR laser (808 nm, 1 W cm⁻²) generated from an MDL-III-808-2.5W laser device (Changchun New Industries Optoelectronics Technology Co., Ltd., Changchun, China) for 9 min. Afterwards, the cells were incubated at 37°C for 24 h. Then, the cells were incubated with 10% CCK-8 for 1 h, and the absorbance intensity at 450 nm was measured with a Microplate Reader (RT-6100, Rayto Life and Analytical Sciences, Shenzhen, China) after shaking for 2 min, using 630 nm as reference wavelength.

2.8. Statistical analysis

All experiments were performed in triplicate. The data were presented as mean ± standard deviation, and were statistically analyzed with SPSS 16.0 software. One-way analysis of variance (ANOVA) followed by Levene's Test for equality of variances as well as Bonferroni multiple comparison test were utilized for the comparison of mean values. A value of $p < 0.05$ was considered as significant.

3. Results and Discussion

3.1. Preparation of CIPN

The CIPN was prepared using PIC method (Fig. 1). It contains nanodroplets composed of PFPE and IR780 as core, and Pluronic and catalase as shell (Fig. 1). Nanoemulsions are transparent or translucent, and kinetically stable colloidal systems having droplet size that ranges from 10 nm to 500 nm.²⁸ Nanoemulsions can be formed using a variety of approaches which are usually categorized as either high-energy methods or low-energy methods.²⁹ High-energy methods utilize the intensive disruptive forces provided by mechanical devices including sonicators, microfluidizers, and high pressure valve homogenizers to generate small droplets. They involve temperature elevation during the preparation process, which may elicit loss of catalase activity and IR780 (which is easily degraded) decomposition. In contrast, low-energy methods including phase inversion temperature (PIT) method and PIC method rely on the spontaneous formation of tiny droplets when the solution or environmental conditions (e.g., composition or temperature) are changed.³⁰ They hold advantages including prevention of catalase destruction and

IR780 decomposition, low cost, low energy consumption, ease in formation, and suitability for industrialization as no expensive equipment is required. In particular, PIC is a very attractive approach because its entire procedure is carried out at room temperature.³¹ The PIC method holds advantage over routine chemical synthetic methods in terms of prevention of catalase activity loss, since catalase activity impairment is a common phenomenon in chemical synthetic approaches and it has been reported that 79% of catalase activity was lost after chemical synthesis.^{32,33} For example, the side chains of catalase were chemically grafted to the chemotherapeutic drug cis-aconitic anhydride-linked doxorubicin, and the catalase activity was decreased after chemical conjugation.¹⁸ It is possible that the chemical conjugation compromised the folding of the peptide chain and consequently influenced the enzymatic activity, since the formation of the enzyme active center requires the correct folding of the peptide chain.

3.2. Characterization of CIPN

IR780, a NIR photodynamic agent, has been intensively studied for PDT owing to its appealing

features including fluorescence imaging ability, specific mitochondria-targeting capability, and preferential accumulation in multiple tumor cells.³⁴ However, the biomedical application of IR780 is hampered by its extremely low aqueous solubility, which weakens the therapeutic efficacy. Herein, we encapsulated IR780 into the nanoemulsion system CIPN. The CIPN exhibited a homogeneous appearance (Fig. 2(a) inset), which indicated the improvement of aqueous solubility. As revealed by dynamic light scattering measurements, the droplet diameter of the CIPN is 192.5 ± 3.83 nm, with polydispersity 0.20 ± 0.07 (Fig. 2(a)). This droplet size is in favor of the preferential accumulation of IR780 in tumor sites, since it has been reported that nanoparticles with the size of 10–400 nm can accumulate in tumor tissue at levels 70 times higher than in normal tissue owing to the enhanced permeability and retention (EPR) effect.^{35,36} The polydispersity values indicate the relatively narrow size distribution. The zeta potential was 2.03 ± 1.41 mV (Fig. 2(b)). The TEM image revealed the spherical morphology of the CIPN, and verified the droplet size results obtained from dynamic light scattering measurements (Fig. 2(c)). Consistent with the green color of the CIPNs

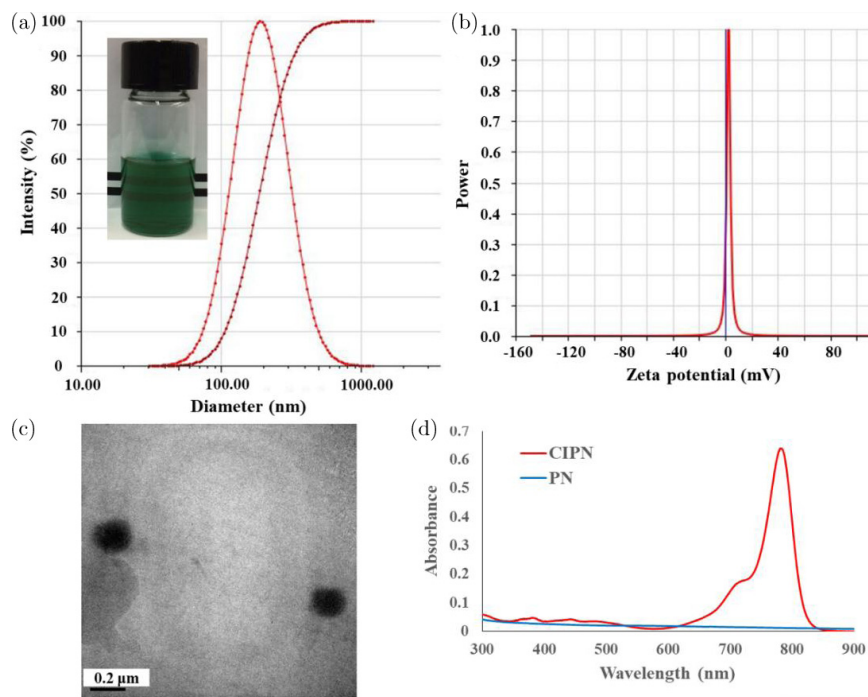


Fig. 2. Characterization of CIPN. (a) Diameter and polydispersity. Inset: Appearance. (b) Zeta potential. (c) Transmission electron microscopy image. (d) Absorbance spectra of diluted PN and CIPN. PN, PFPE/water nanoemulsion. CIPN, catalase@IR780-PFPE/water nanoemulsion.

(Fig. 2(a) inset), the absorption spectrum of CIPN presented strong absorption around 780 nm, while PN showed no absorption (Fig. 2(d)). This suggests the successful encapsulation of IR780 into the nanoemulsion system. The encapsulation of IR780 into the nanodroplets with an average diameter of less than 200 nm has the potential to achieve sustained drug release in physiological conditions, since it has been reported that polymeric nanoparticles³⁷ and liposomes²⁰ with similar particle size ($> 200 \text{ nm}$) showed sustained drug release. The sustained release may decrease the drug administration frequency and reduce drug side effects.

Stability of nanomaterials in physiological solutions is essential for their biomedical application. The CIPNs showed neither precipitation nor fluctuations in the mean droplet diameters ($p > 0.05$) after being incubated in cell culture medium for up to 48 h at both 25°C and 37°C (Fig. 3), indicating their satisfactory stability in a physiological environment. Particularly, it was observed that after storage at 4°C for 15 months, the IPN showed obvious precipitation, while the CIPN retained its homogeneous appearance (Fig. S1). This suggests that the catalase coated the droplets and consequently increased the stability. To further elucidate the function of catalase in the nanodroplet formation, we investigated the IR780 encapsulation efficiency and loading capacity of IPN and CIPN. The CIPN showed improved encapsulation efficiency (2.4 fold) and loading capacity (2.3 fold) in comparison with IPN (Table 1). This suggests that catalase facilitated the IR780 encapsulation into the nanoemulsion system. The reason for this phenomenon may be that catalase, as a kind of protein, has

both hydrophobic amino acids and hydrophilic amino acids, and may facilitate the assembly of nanodroplets.

3.3. Photodynamic efficacy in aqueous solution

To evaluate the ability of the CIPN to decompose tumor endogenous H₂O₂ and improve PDT efficiency, the ¹O₂ production of the CIPN and IPN with the same IR780 concentration was quantified using a specific ¹O₂ probe DPBF. As soon as the CIPN was added into the H₂O₂ solution, numerous oxygen bubbles were generated. Even after minutes, a lot of oxygen bubbles could be seen (Fig. 4 inset). In contrast, the IPN showed no oxygen generation when it was mixed with H₂O₂ solution. This suggests that the CIPN could generate oxygen efficiently in response to tumor endogenous H₂O₂ owing to the strong enzymatic activity of catalase. Consistently, the CIPN produced remarkably higher level of ¹O₂ than the IPN under excitation by NIR light (Fig. 4), suggesting the ability of CIPNs to boost PDT efficiency and thereby improve therapeutic outcomes via augmenting oxygen supply in the presence of H₂O₂. In particular, in the absence of H₂O₂, the CIPN could not generate oxygen or change the ¹O₂ efficiency in comparison with the IPN (Fig. 4). This highlights the high tumor selectivity of the CIPN, which facilitates the prevention of damage to adjacent healthy tissues. Apart from the EPR effect rendered by the nano-range size of the CIPN, the tumor specificity can be further enhanced by the presence of catalase.³⁵ Similarly, liposomes co-loading catalase and photosensitizer were reported to improve ROS generation and PDT efficiency via additional oxygen supply.²⁰ It has also been reported that catalase-loaded nanoformulation improved ROS generation under hypoxic experimental conditions.¹⁸

3.4. Cytocompatibility

Good cytocompatibility of a nanoformulation in darkness facilitates the tumor targeting effect of PDT, since in this way, the tissue area that exhibits toxic effects would be only the light-illuminated region. To evaluate the cytocompatibility of the CIPNs, CCK-8 assay was used to assess the viabilities of OVCAR-3 cells incubated with different

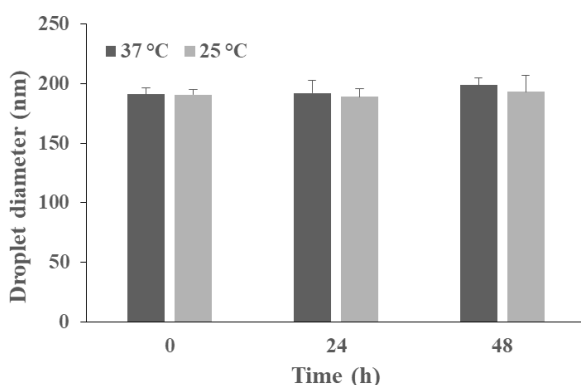


Fig. 3. Mean droplet diameters of the CIPNs during storage at 37°C or 25°C for up to 48 h. CIPN, catalase@IR780-PFPE/water nanoemulsion.

Table 1. Encapsulation efficiency and loading capacity of PN and CIPN.

	Encapsulation efficiency (%)	Loading capacity (%)
CIPN	6.57 ± 0.75	0.07 ± 0.006
PN	2.69 ± 0.53	0.03 ± 0.005

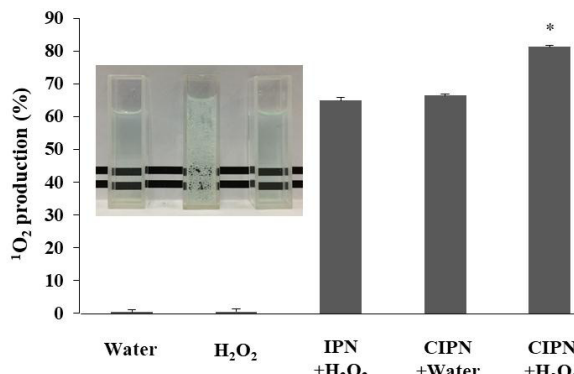


Fig. 4. The production of $^1\text{O}_2$ from IPN or CIPN having the same IR780 concentration in the presence or absence of H_2O_2 under NIR light irradiation. The inset is a photo of the mixture of IPN and H_2O_2 solution (left), CIPN and H_2O_2 solution (middle), and CIPN and water (right). *indicates a significant difference in comparison with the IPN + H_2O_2 group (significance level = 0.05, n = 3). $^1\text{O}_2$, singlet oxygen. IPN, IR780-PFPE/water nanoemulsion. CIPN, catalase@IR780-PFPE/water nanoemulsion.

concentrations (25–800 $\mu\text{g mL}^{-1}$) of CIPNs without exposure to light for 24 h. No toxicity was detected even at the concentration as high as 800 $\mu\text{g mL}^{-1}$ (Fig. 5). This suggests the satisfactory biocompatibility of CIPN.

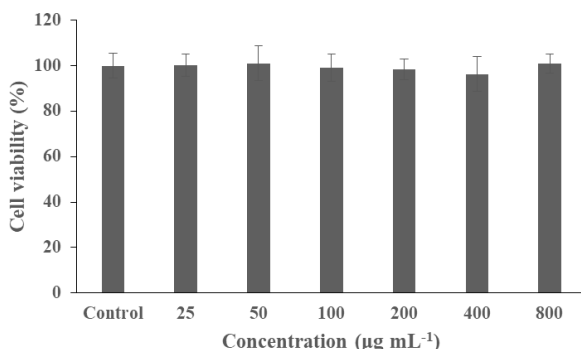


Fig. 5. Viabilities of OVCAR-3 cells after incubation with different concentrations of CIPNs for 24 h in dark. The concentration was calculated as the weight of the entire nano-droplet including pluronic and PFPE divided by total volume. CIPN, catalase@IR780-PFPE/water nanoemulsion.

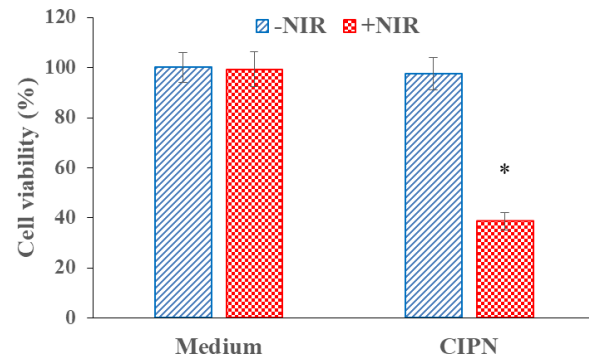


Fig. 6. Cell viabilities of OVCAR-3 cells treated with culture medium or CIPNs with/without NIR light irradiation. *indicates significant difference compared with the Medium + NIR group ($p < 0.05$, n = 3). CIPN denotes catalase@IR780-PFPE/water nanoemulsion. NIR denotes near-infrared.

3.5. In vitro PDT

To evaluate the ability of the CIPN to kill cancer cells in response to light stimulation, we measured the viabilities of OVCAR-3 cells incubated with culture medium or CIPN with and without 808 nm laser irradiation using CCK-8 cell viability assay. As shown in Fig. 6, cells treated without CIPN and with NIR irradiation showed little viability alteration ($p > 0.05$), which suggested that the light irradiation density and dose used in the test could not generate damage to the cells. In contrast, under the same NIR irradiation condition, cells incubated with CIPNs presented a sharp decrease of cell viability to $\sim 39\%$. This demonstrates the CIPNs could efficiently kill cancer cells in response to light irradiation. Moreover, cells incubated with CIPNs in dark showed no cell viability change, demonstrating that the cell destruction was a combination effect of CIPNs and NIR light. In a word, the results suggest that the CIPN may be an efficient NIR-activatable nanoformulation for cancer therapy. Nevertheless, further studies under hypoxic experimental condition remain to be explored to fully demonstrate the potential of the CIPN to serve as a highly efficient cancer photo-therapeutic.

4. Conclusion

We rationally designed a nanoplatform CIPN, which could combine the merits of *in situ* oxygen generation strategy and oxygen delivery strategy to relieve tumor hypoxia and boost the therapeutic efficiency of NIR light-mediated PDT. This concisely prepared CIPN contains catalase that could

decompose tumor endogenous H₂O₂ to generate oxygen, PFPE with superior oxygen loading capacity, and a NIR photosensitizer IR780. It presented augmented and H₂O₂-controllable generation of ¹O₂ under light irradiation, excellent cytocompatibility, and ability to kill cancer cells in response to NIR light stimulation. Integrating the high tumor specificity of *in situ* oxygen generation strategy and high efficiency of oxygen delivery strategy, the CIPN provides opportunity for the design of nanomedicine for efficient and selective NIR light-triggered hypoxic tumor therapy.

Conflict of Interest

The authors declare no conflicts of interest.

Acknowledgments

This work was supported by the National Natural Science Foundation of China (61525503/61835009/61722508/61935012/61620106016), (Key) Project of Department of Education of Guangdong Province (2016KCXTD007), and Shenzhen Science and Technology Funding (JCYJ20180305124902165/JCYJ20170412105003520). TEM analysis was supported by the Instrumental Analysis Center of Shenzhen University.

References

1. J. Tian, B. Huang, M. H. Nawaz, W. Zhang, "Recent advances of multi-dimensional porphyrin-based functional materials in photodynamic therapy," *Coord. Chem. Rev.* **420**, 213410 (2020).
2. H. Chen, C. He, T. Chen, X. Xue, "New strategy for precise cancer therapy: tumor-specific delivery of mitochondria-targeting photodynamic therapy agents and *in situ* O₂-generation in hypoxic tumors," *Biomater. Sci.* **8**(14), 3994–4002 (2020).
3. M. Hockel, P. Vaupel, "Tumor hypoxia: Definitions and current clinical, biologic, and molecular aspects," *JNCI-J. Natl. Cancer Inst.* **93**(4), 266–276 (2001).
4. X. Li, J. Wang, R. Cui, D. Xu, L. Zhu, Z. Li, H. Chen, Y. Gao, L. Jia, "Hypoxia/pH dual-responsive nitroimidazole-modified chitosan/rose bengal derivative nanoparticles for enhanced photodynamic anti-cancer therapy," *Dyes Pigment.* **179**, 108395 (2020).
5. J. M. Brown, W. R. Wilson, "Exploiting tumour hypoxia in cancer treatment," *Nat. Rev. Cancer* **4**(6), 437–447 (2004).
6. A. L. Harris, "Hypoxia — a key regulatory factor in tumour growth," *Nat. Rev. Cancer* **2**(1), 38–47 (2002).
7. B. Yang, Z. Dai, G. Zhang, Z. Hu, X. Yao, S. Wang, Q. Liu, X. Zheng, "Ultrasmall ternary FePtMn nanocrystals with acidity-triggered dual-ions release and hypoxia relief for multimodal synergistic chemodynamic/photodynamic/photothermal cancer therapy," *Adv. Healthc. Mater.* **9**(21), 1901634 (2020).
8. X. Liu, G. Li, M. Xie, S. Guo, W. Zhao, F. Li, S. Liu, Q. Zhao, "Rational design of type I photosensitizers based on Ru(II) complexes for effective photodynamic therapy under hypoxia," *Dalton Trans.* **49**(32), 11192–11200 (2020).
9. J. Chen, H. Luo, Y. Liu, W. Zhang, H. Li, T. Luo, K. Zhang, Y. Zhao, J. Liu, "Oxygen-self-produced nanoplateform for relieving hypoxia and breaking resistance to sonodynamic treatment of pancreatic cancer," *ACS Nano* **11**(12), 12849–12862 (2017).
10. Y. Cheng, H. Cheng, C. Jiang, X. Qiu, K. Wang, W. Huan, A. Yuan, J. Wu, Y. Hu, "Perfluorocarbon nanoparticles enhance reactive oxygen levels and tumour growth inhibition in photodynamic therapy," *Nat. Commun.* **6**, 8785 (2015).
11. B. Pucelik, A. Sufek, A. Barzowska, J. M. Dabrowski, "Recent advances in strategies for overcoming hypoxia in photodynamic therapy of cancer," *Cancer Lett.* **492**, 116–135 (2020).
12. N. Yang, W. Xiao, X. Song, W. Wang, X. Dong, "Recent advances in tumor microenvironment hydrogen peroxide-responsive materials for cancer photodynamic therapy," *Nano-Micro Lett.* **12**(1), 15 (2020).
13. Q. He, H. Hu, Q. Zhang, T. Wu, Y. Zhang, K. Li, C. Shi, "Ultra-dispersed biomimetic nanoplateform fabricated by controlled etching agglomerated MnO₂ for enhanced photodynamic therapy and immune activation," *Chem. Eng. J.* **397**, 125478 (2020).
14. Q. Chen, L. Feng, J. Liu, W. Zhu, Z. Dong, Y. Wu, Z. Liu, "Intelligent albumin–MnO₂ nanoparticles as pH-/H₂O₂-responsive dissociable nanocarriers to modulate tumor hypoxia for effective combination therapy," *Adv. Mater.* **28**(33), 7129–7136 (2016).
15. B. Huang, S. Chen, W. Pei, Y. Xu, Z. Jiang, C. Niu, L. Wang, "Oxygen-sufficient nanoplateform for chemo-sonodynamic therapy of hypoxic tumors," *Front. Chem.* **8**, 358 (2020).
16. X. Li, H. Yu, Y. Huang, Y. Chen, J. Wang, L. Xu, F. Zhang, Y. Zhuge, X. Zou, "Preparation of microspheres encapsulating sorafenib and catalase and their application in rabbit VX2 liver tumor," *Biomed. Pharmacother.* **129**, 110512 (2020).

17. X. Liu, Q. Wang, H. Zhao, L. Zhang, Y. Su, Y. Lv, "BSA-templated MnO₂ nanoparticles as both peroxidase and oxidase mimics," *Analyst* **137**(19), 4552–4558 (2012).
18. X. Cheng, L. He, J. Xu, Q. Fang, L. Yang, Y. Xue, X. Wang, R. Tang, "Oxygen-producing catalase-based prodrug nanoparticles overcoming resistance in hypoxia-mediated chemo-photodynamic therapy," *Acta Biomater.* **112**, 234–249 (2020).
19. Y. Fan, S. Guan, W. Fang, P. Li, B. Hu, C. Shan, W. Wu, J. Cao, B. Cheng, W. Liu, Y. Tang, "A smart tumor-microenvironment responsive nanoprobe for highly selective and efficient combination therapy," *Inorg. Chem. Front.* **6**(12), 3562–3568 (2019).
20. L. Deng, D. Sheng, M. Liu, L. Yang, H. Ran, P. Li, X. Cai, Y. Sun, Z. Wang, "A near-infrared laser and H₂O₂ activated bio-nanoreactor for enhanced photodynamic therapy of hypoxic tumors," *Biomater. Sci.* **8**(3), 858–870 (2020).
21. M. Li, Y. Shao, J. H. Kim, Z. Pu, X. Zhao, H. Huang, T. Xiong, Y. Kang, G. Li, K. Shao, J. Fan, J. W. Foley, J. S. Kim, X. Peng, "Unimolecular photodynamic O₂-economizer to overcome hypoxia resistance in phototherapeutics," *J. Am. Chem. Soc.* **142**(11), 5380–5388 (2020).
22. Z. Zhou, B. Zhang, H. Wang, A. Yuan, Y. Hu, J. Wu, "Two-stage oxygen delivery for enhanced radiotherapy by perfluorocarbon nanoparticles," *Theranostics* **8**(18), 4898–4911 (2018).
23. X. Li, N. Kwon, T. Guo, Z. Liu, J. Yoon, "Innovative strategies for hypoxic-tumor photodynamic therapy," *Angew. Chem.-Int. Edit.* **57**(36), 11522–11531 (2018).
24. X. Shi, Q. Zhan, X. Yan, J. Zhou, L. Zhou, S. Wei, "Oxyhemoglobin nano-recruiter preparation and its application in biomimetic red blood cells to relieve tumor hypoxia and enhance photodynamic therapy activity," *J. Mat. Chem. B* **8**(3), 534–545 (2020).
25. P. W. Buehler, Y. Zhou, P. Cabrales, Y. Jia, G. Sun, D. R. Harris, A. G. Tsai, M. Intaglietta, A. F. Palmer, "Synthesis, biophysical properties and pharmacokinetics of ultrahigh molecular weight tense and relaxed state polymerized bovine hemoglobins," *Biomaterials* **31**(13), 3723–3735 (2010).
26. L. Yao, L. Feng, D. Tao, H. Tao, X. Zhong, C. Liang, Y. Zhu, B. Hu, Z. Liu, Y. Zheng, "Perfluorocarbon nanodroplets stabilized with cisplatin-prodrug-constructed lipids enable efficient tumor oxygenation and chemo-radiotherapy of cancer," *Nanoscale* **12**(27), 14764–14774 (2020).
27. K. de Oliveira Gonçalves, D. P. Vieira, L. C. Courrol, "Synthesis and characterization of aminolevulinic acid gold nanoparticles: Photo and sonosensitizer agent for atherosclerosis," *J. Lumines.* **197**, 317–323 (2018).
28. L. Hong, C. L. Zhou, F. P. Chen, D. Han, C. Y. Wang, J. X. Li, Z. Chi, C. G. Liu, "Development of a carboxymethyl chitosan functionalized nanoemulsion formulation for increasing aqueous solubility, stability and skin permeability of astaxanthin using low-energy method," *J. Microencapsul.* **34**(8), 707–721 (2017).
29. A. K. Das, P. K. Nanda, S. Bandyopadhyay, R. Banerjee, S. Biswas, D. J. McClements, "Application of nanoemulsion-based approaches for improving the quality and safety of muscle foods: A comprehensive review," *Compr. Rev. Food. Sci. Food Saf.* **19**(5), 2677–2700 (2020).
30. D. J. McClements, "Edible nanoemulsions: fabrication, properties, and functional performance," *Soft Matter* **7**(6), 2297–2316 (2011).
31. F. Hansali, M. Wu, D. Bendedouch, E. Marie, "n-Butyl cyanoacrylate miniemulsion polymerization via the phase inversion composition method," *Colloid Surf. A-Physicochem. Eng. Asp.* **393**, 133–138 (2012).
32. Q. Chen, J. Chen, C. Liang, L. Feng, Z. Dong, X. Song, G. Song, Z. Liu, "Drug-induced co-assembly of albumin/catalase as smart nano-theranostics for deep intra-tumoral penetration, hypoxia relieve, and synergistic combination therapy," *J. Control. Release* **263**, 79–89 (2017).
33. G. Song, Y. Chen, C. Liang, X. Yi, J. Liu, X. Sun, S. Shen, K. Yang, Z. Liu, "Catalase-loaded TaOx nanoshells as bio-nanoreactors combining high-Z element and enzyme delivery for enhancing radiotherapy," *Adv. Mater.* **28**(33), 7143–7148 (2016).
34. X. Tan, S. Luo, D. Wang, Y. Su, T. Cheng, C. Shi, "A NIR heptamethine dye with intrinsic cancer targeting, imaging and photosensitizing properties," *Biomaterials* **33**(7), 2230–2239 (2012).
35. M. E. Davis, Z. Chen, D. M. Shin, "Nanoparticle therapeutics: an emerging treatment modality for cancer," *Nat. Rev. Drug Discov.* **7**(9), 771–782 (2008).
36. F. Alexis, E. Pridgen, L. K. Molnar, O. C. Farokhzad, "Factors affecting the clearance and biodistribution of polymeric nanoparticles," *Mol. Pharm.* **5**(4), 505–515 (2008).
37. P. Zhang, S. R. Zhao, J. X. Li, L. Hong, M. A. Raja, L. J. Yu, C. G. Liu, "Nanoparticles based on phenylalanine ethyl ester-alginate conjugate as vitamin B₂ delivery system," *J. Biomater. Appl.* **31**(1), 13–22 (2016).